A Novel Robotic Guidance System with Eye Gaze Tracking Control for Needle based Interventions

Jing Guo, Yi Liu, Qing Qiu, Jie Huang, Chao Liu, Zhiguang Cao, Yue Chen

▶ **To cite this version:**

Jing Guo, Yi Liu, Qing Qiu, Jie Huang, Chao Liu, et al.. A Novel Robotic Guidance System with Eye Gaze Tracking Control for Needle based Interventions. IEEE Transactions on Cognitive and Developmental Systems, 2021, 13 (1), pp.179-188. 10.1109/TCDS.2019.2959071 . lirmm-03069985

HAL Id: lirmm-03069985

https://hal-lirmm.ccsd.cnrs.fr/lirmm-03069985

Submitted on 7 Sep 2022

HAL is a multi-disciplinary open access archive for the deposit and dissemination of scientific research documents, whether they are published or not. The documents may come from teaching and research institutions in France or abroad, or from public or private research centers.

L'archive ouverte pluridisciplinaire **HAL**, est destinée au dépôt et à la diffusion de documents scientifiques de niveau recherche, publiés ou non, émanant des établissements d'enseignement et de recherche français ou étrangers, des laboratoires publics ou privés.

A Novel Robotic Guidance System With Eye-Gaze Tracking Control for Needle-Based Interventions

Jing Guo, Yi Liu, Qing Qiu, Jie Huang, Chao Liu, *Senior Member, IEEE*, Zhiguang Cao, and Yue Chen, *Member, IEEE*

***Abstract*—The robotic technologies have been widely used in the operating room for decades. Among them, needle-based percutaneous interventions have attracted much attention from engineering and medical communities. However, the currently used robotic systems for interventional procedures are too cumbersome, requiring a large footprint in the operating room. Recently developed light-weight puncture robotic systems for needle positioning are able to reduce the size, but has the limitation of awkward ergonomics. In this article, we design a compact robotic guidance system that could accurately realize the needle position and orientation within the operating room. The eye-gaze tracking-based approach is proposed to control the position and orientation of the needle toward the desired location in a more intuitive manner, and the forward and inverse kinematics of this 4-DoF robot are analyzed. The robot operating system (ROS)-based experimental studies are performed to evaluate the needle placement accuracy during interventional therapy. The result indicated the effectiveness of the proposed robotic hardware and the eye-gaze-based control framework, which can achieve a distance error of the robot's end effector to the target point within 1 mm.**

***Index Terms*—Eye-gaze tracking, needle guidance, percutaneous interventions, surgical robot.**

I. Introduction

PUNCTURE needle intervention has shown to be an effective and minimally invasive approach for biopsy [1], tumor ablation [2], and brachytherapy [3]. To perform this procedure, the radiologist manually maneuvers the needles toward the target location under various image feedback (i.e., ultrasound, flouroscope, and MRI). The success rate of this procedure highly relies on the manipulation precision of the administering radiologist. For the un-experienced operator, high tension and long procedural time are often inevitable in the realistic procedures. Thus, a variety of approaches have been proposed to improve the treatment performance, such as deploying the needle under real-time image feedback, various motion compensation methods for abdomen percutaneous procedures, and using robotic platform for the needle insertions.

Compared to the manual approach, robot-assisted needle insertion is able to provide enhanced position and orientation accuracy since the needle pose with respect to target can be accurately calculated from the kinematics modeling. Prior to the percutaneous procedures, the robot is registered with the medical image coordinate frame via a rigid body transformation method [4]. To move the robot toward the target location, the robot control algorithm reads the command send from the radiologist (i.e., joystick or haptic interface) and move each joints of the robot with joint-space feedback such as encoders. Task-space closed-loop control can be achieved via the intraoperative image feedback to achieve superior targeting performance (see recent work in various robot-assisted needle insertions [5]–[12]).

Based on the task of surgical intervention performed by the robot, general robotic systems for percutaneous needle procedures are composed of at least two modules: 1) needle pose and 2) needle insertion. An accurate needle pose control is crucial for the safety and effectiveness of the procedure, which moves the tip of the needle at the skin entry point as well as orients the needle shaft to the desired insertion direction. After the needle achieves the desired pose, the insertion module is used to push the needle to the desired target. However, for the sake of safety, the insertion module is usually not favored by the clinician. The "surgeon in the loop" design is developed to assist the operation only by needle position module as indicated in [13]–[18]. Consequently, the clinician can use the robot to position the needle with the guidance from the medical image by either teleoperated or image-guided approach, then manually insert the needle to the target.

The teleoperated approach is usually used in robotic-assisted surgery, in which the clinician operates the robotic system via joystick or GUI [19]–[21]. In order to improve the

Manuscript received July 30, 2019; revised November 30, 2019; accepted December 6, 2019. Date of publication December 12, 2019; date of current version March 11, 2021. This work was supported in part by the National Natural Science Foundation of China through Guangzhou Elite Project under Grant 61803103, in part by the National Natural Science Foundation of China under Grant 51605098, in part by the Singapore National Research Foundation under Grant NRF-RSS2016-004, and in part by the International Science and Technology Cooperation Program of Guangzhou under Grant 201807010006. *(Corresponding authors: Jie Huang; Zhiguang Cao.)*

J. Guo, Y. Liu, and Q. Qiu are with the School of Automation, Guangdong University of Technology, Guangzhou 510006, China (e-mail: toguojing@gmail.com; yi_liu@mail2.gdut.edu.cn; qiuqing@mail2.gdut.edu.cn).

J. Huang is with the Guangdong Lung Cancer Institute, Guangdong Provincial Key Laboratory of Translational Medicine in Lung Cancer, Guangdong Provincial People's Hospital, Guangdong Academy of Medical Sciences, Guangzhou, China, and also with the Guangdong Academy of Medical Sciences, Guangzhou 510080, China (e-mail: jieh2015@yahoo.com).

C. Liu is with the Department of Robotics, LIRMM-CNRS, 34095 Montpellier, France (e-mail: liu@lirmm.fr).

Z. Cao is with the Department of Industrial Systems Engineering and Management, National University of Singapore, Singapore (e-mail: isecaoz@nus.edu.sg).

Y. Chen is with the Mechanical Engineering, University of Arkansas, Fayetteville, AR 72701 USA (e-mail: yc039@uark.edu).

Color versions of one or more of the figures in this article are available online at https://ieeexplore.ieee.org.

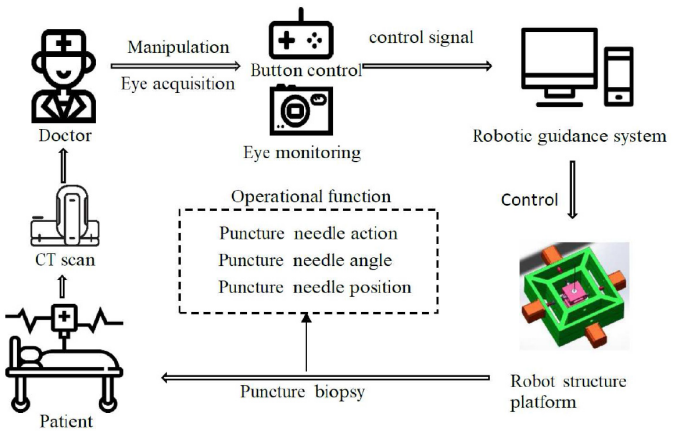

Fig. 1. Environed schematic diagram of the puncture robotic system. The doctor controls the robot to change the pose of the puncture sheath.

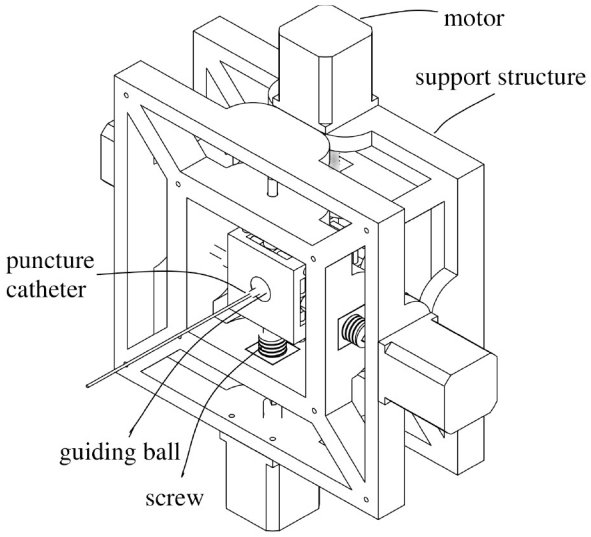

Fig. 2. Assembly view of the robot. The robot consists of two layers and controls the needle pose by the combination of two layers of movement.

performance of the teleoperation system, some advanced methods have been proposed in [22]–[26]. The bilateral teleoperation system is designed to conduct the remote sensing for the operator, thus the clinician can obtain the remote environment interaction information. Some recent work for bilateral teleoperation can be found in [27]–[29]. Even if the teleoperated configuration is common in the robotic-assisted surgery, it is noticed that sometimes the hand of the clinician might be occupied by other medical devices, which make it difficult to manipulate the joystick or other devices to teleoperate the robot at the same time. Moreover, in the case of switching between the joystick/control devices and surgical tools (i.e., needles), necessary sterilization of the clinician must be performed, which often makes the procedures longer than expected. And the way to control medical devices through the joystick or GUI requires a lot of training costs for doctors to master complex robot systems. Therefore, it will be interesting to improve the human–robot interaction method that allows the clinician to control the robot for needle pose directly while allowing other tasks to be performed at the same time in the operating room. In [30], an eye-tracking device is used with the attempt to control the robotic arm, but these expensive eye-tracking devices do not provide tracking accuracy that matches the device price enough, besides that the mounted glass may hinder the operation of the clinician. In [31], a deep convolutional neural-network-based gaze direction classification method with face detection is implemented with RGB camera to control the surgical robot. However, no further evaluation of the specific surgical procedures was performed or indicated [31]. To reduce the above-mentioned training costs for clinician operating the robot systems and improve the equipment performance, in this article, we present a novel lightweight robotic guidance system for percutaneous procedures. This robot is powered with four high-performance motors to provide the necessary needle position and orientation control. In order to improve the human–robot interaction, an eye-gaze tracking method is proposed, with which the radiologist can control the needle pose with eye gaze. The control framework of the proposed system can be seen in Fig. 1, and the contribution of this article includes the following.

1) The novel robotic system mechanical design and modeling. The prototype has the potential to be further improved to create a body-mounted robot.
2) An intuitive control approach with eye-gaze tracking is designed, which enables the eye movement to control the needle pose during the procedure.
3) The proposed eye-hand collaborative control framework helps the clinician to perform the needle positioning without sterilization issues, especially when the hand of the operator needs to be switched between control devices and surgical tools.

The structure of this article is as follows. Section II introduces the robot mechanical design and kinematic modeling. Section III presents the eye-gaze-tracking-based control for the proposed robotic system. Section IV details the experimental study and result analysis followed by the conclusion in Section V.

II. Robot Design and Modeling

A. Mechanical Design

The assembly view of the proposed robot is shown in Fig. 2, which shows that, two parallel blocks are connected through the lead screw and the bearing, guiding balls are also designed to connect the blocks. Two guiding balls are used to connect the puncture sheath, and the needle is subjected to a constraint through the puncture sheath. When the lead screw is rotated, the block translates linearly. Due to relative displacement between the upper and lower layers, the direction of the puncture sheath can be accurately tilted, leads to the needle orientation control during the puncture operation. To ensure that the parallel blocks can move simultaneously without changing the angle of the puncture sheath, a margin of the reservation is placed between the two parallel blocks and the support structure.

The rotation of the puncture sheath relies on the translation of the two blocks in the designed robot. As shown in Fig. 3,

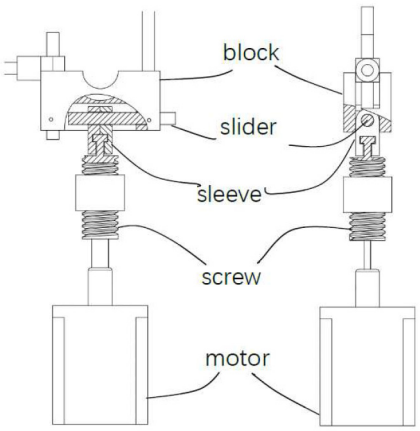

Fig. 3. Details of the robot's structure, the motor is connected to the lead screw, and the lead screw is connected to the block through the sleeve. The rotation angle of the motor is controlled to control the linear movement of the lead screw relative to the fixed support structure to push the block to move.

we can control the parallel blocks to slide at the same time. In the designed robot, a lead screw drive structure is used to drive the lead screw to move horizontally by rotating the motor (rotation angle β), thus translates the block through the connecting rod. Transnational distance d of the block can be obtained as follows:

$$d = k\beta \tag{1}$$

where k is the transmission ratio of the lead screw that is determined by the pitch of the lead screw. Fig. 4(a) shows the detailed description and the corresponding parameters of the designed robot. The control of the guiding ball rotation is affected by the virtual joint of the robot. Hence, the guiding ball can be rotated by the two motors at angle θ or move the length d in the horizontal direction. As the needle passing through both layers, its orientation can be controlled by translating one layer with the other, as depicted in Fig. 4(b), where the puncture sheath joint rotates with certain angle to accommodate the movement of the block via the mechanical design of the robot.

The end effector of the robot is a 4-DoF puncture sheath that is controlled by four motors, and the puncture sheath can be moved horizontally in a small range or rotated at a certain angle to change the pose of the end effector. The kinematics of the robot is built via novel design of the mechanical structure. The top corner of the support structure is defined as the origin of the coordinate of the robot, and the initial coordinate of the center of the upper block is the fixed coordinate point of the puncture sheath. In practice, the position of the target can be calibrated by two cameras whose imaging angles are perpendicular to each other. In Fig. 4, only the YZ plane of the camera angle of view is provided, in which Fig. 4(a) shows the coordinate relationship when the two blocks keep the initial state and there is no movement and rotation of the puncture sheath; in Fig. 4(b), the lower block moves with distance d thus the value of the movement can be calculated by (1). The puncture sheath only rotates angle θ in the YZ coordinate system, and the origin of the puncture sheath coordinate will not be changed at this moment. The initial length of

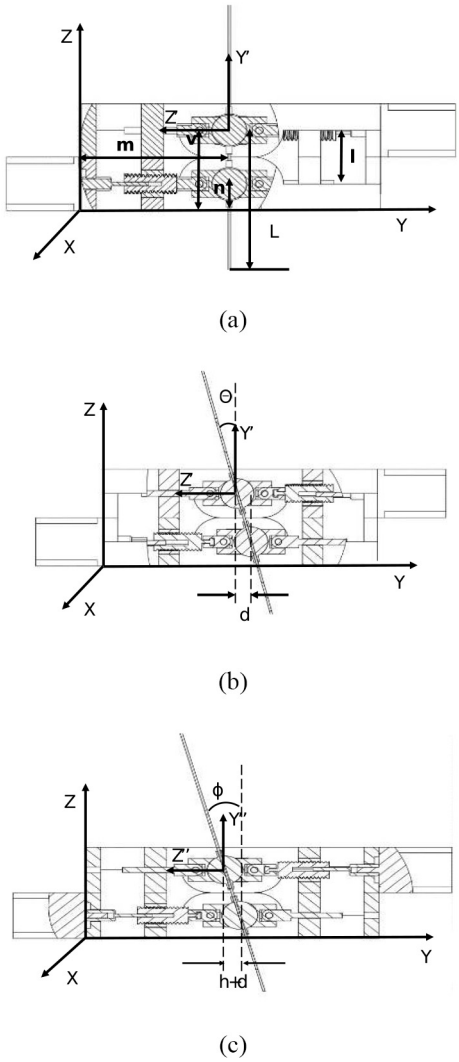

Fig. 4. 2-D model of the robot. Each block is controlled by two motors to move in a straight line in the XY plane. The puncture sheath determines the angle and direction of rotation through the two blocks and the guiding ball, thus the puncture sheath has four degrees of freedom of direction. (a) In the initial state, the puncture sheath is perpendicular to the world coordinate XY plane and the puncture sheath coordinate origin is unchanged. (b) Only the lower block is moved to change the direction of the puncture sheath, and the puncture sheath coordinate origin is unchanged. (c) Move the upper and lower blocks at the same time, and the origin of the puncture sheath coordinates changes.

the simulated puncture needle L will not be affected during the rotation, and the vertical distance l between the two parallel blocks is constant. Therefore, the rotation angle θ required for the puncture needle can be calculated by the block movement distance d and l, and the puncture sheath performs puncture after the rotation motion. The initial height H_L of the needle is calculated as follows:

$$\theta = \frac{\pi}{2} - \arctan\left(\frac{l}{d}\right) \tag{2}$$

$$H_L = L(1 - \cos(\theta)). \tag{3}$$

During the operation, the position of the target may change due to the doctor's judgment, so it is necessary to move the original position of the puncture sheath to change the needle position to follow the target. The block with the origin of

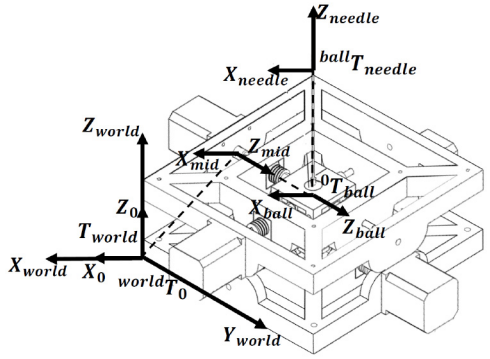

Fig. 5. Transfer matrix relationship of the robot.

the puncture sheath can be moved so that a larger inclination angle φ can be induced. Different from the origin of the puncture sheath coordinate in Fig. 4(b), the upper block in Fig. 4(c) can move to generate larger angle further to make the puncture sheath to translate certain distance. In this way, the puncture sheath can be shifted by h with respect to the world coordinate system. The needle insertion position will be changed when the coordinate position of the support structure is constant in this case. Therefore, it is necessary to compensate the movement of the block considering its origin coordinate by moving the support structure to ensure that the coordinates of the origin of the puncture sheath keeps still with the world coordinate system.

B. Kinematics Analysis

In this section, the kinematics of the guiding robot is performed based on the world coordinate within XY plane as shown in Fig. 5. T_{needle} is defined as the puncture needle coordinate transformation matrix that can be obtained through homogeneous approach with respect to the world coordinate matrix as defined as T_{world}, where T_{world} is a 4×4 identity matrix. Moreover, the $X_{\text{mid}} - Z_{\text{mid}}$ coordinate system is the transformation of the virtual joint with consideration of the world coordinate T_{world}, and the transformation matrix ${}^0T_{\text{ball}}$ can be obtained as follows:

$$
\begin{aligned}
{}^{\text{world}}T_0 &= T_{\text{world}} \\
{}^0T_{\text{ball}} &= \begin{bmatrix} 1 & 0 & 0 & x' + \Delta x \\ 0 & 0 & 1 & y' + \Delta y \\ 0 & -1 & 0 & z' \\ 0 & 0 & 0 & 1 \end{bmatrix} \\
{}^{\text{ball}}T_{\text{needle}} &= \begin{bmatrix} \mathbf{R}_{\text{needle}} & \mathbf{P}_{\text{needle}} \\ \mathbf{0} & \mathbf{1} \end{bmatrix} \\
\mathbf{R}_{\text{needle}} &= \begin{bmatrix} \cos\theta_2 & 0 & \sin\theta_2 \\ \sin\theta_2 \sin\theta_1 & \cos\theta_1 & -\sin\theta_1 \cos\theta_2 \\ -\sin\theta_2 \cos\theta_1 & \sin\theta_1 & \cos\theta_1 \cos\theta_2 \end{bmatrix} \\
\mathbf{P}_{\text{needle}} &= \begin{bmatrix} 0 \\ -L\sin\theta_1 \\ L\cos\theta_1 \end{bmatrix}
\end{aligned}
$$

where θ_1 is the rotation angle in the Y_{ball}-axis direction; θ_2 is the rotation angle in the X_{ball}-axis direction; x', y', and z' represent the position relationship of the puncture sheath coordinate system with respect to the world coordinate T_{world}; and Δx and Δy are the distances that the block moves on the X–Y world coordinate T_{world}. Furthermore, the following relationships can obtained:

$$x' = -m \tag{4}$$

$$y' = m \tag{5}$$

$$z' = v \tag{6}$$

$$\theta_1 = \frac{\pi}{2} - \arctan\left(\frac{l}{\Delta x}\right) \tag{7}$$

$$\theta_2 = \frac{\pi}{2} - \arctan\left(\frac{l}{\Delta y}\right) \tag{8}$$

$$\Delta x = x_{\text{low}} + x_{\text{high}} \tag{9}$$

$$\Delta y = y_{\text{low}} + y_{\text{high}} \tag{10}$$

in which x_{low} and y_{low} are the displacements of the lower block in the XY plane, and x_{high} and y_{high} are the displacements of the upper block in the XY plane.

1) Forward Kinematics: The forward kinematics of the robot can be calculated to get the pose of the puncture needle, which is determined by the world coordinate and can be obtained as follows:

$$T_{\text{needle}} = {}^{\text{world}}T_0^0 T_{\text{ball}}^{\text{ball}} T_{\text{needle}}. \tag{11}$$

The pose of puncture needle T_{needle} can be expressed through y_{low}, y_{high}, x_{low}, and x_{high}, which are calculated by the rotation angle of motors through (1).

2) Inverse Kinematics: When the position of the target is known, inverse kinematics should be performed to obtain the desired position of each motor in the robot system. The needle pose depends on the puncture sheath pose, and two parallel blocks control the pose of puncture sheath. Due to the margin of reservation between the parallel blocks and support structure, a variety of analytical solutions are produced. Therefore, there is a threshold of the angle change for the inverse kinematics depending on the coordinate position of the puncture sheath. In this analysis, only the YZ plane is considered, as the XZ plane can be derived in the similar approach. When the rotation angle θ_{target} of the puncture sheath will not exceed the maximum rotation angle θ_{boundary}, the coordinate position of the puncture sheath is fixed. In this case, only the movement of lower block can achieve the change angle of the puncture sheath as indicated

$$\begin{cases} \Delta y = y_{\text{low}} \\ y_{\text{low}} = \dfrac{l}{\tan\theta_{\text{target}}}, \quad \text{if } \theta_{\text{boundary}} > \theta_{\text{target}} \\ y_{\text{high}} = 0. \end{cases} \tag{12}$$

Once the required rotation angle of the puncture sheath exceeds the maximum rotation angle θ_{boundary}, the upper block will move to the required target angle θ, and the position of the puncture sheath coordinate relative to the fixed coordinate system can be compensated by changing the position of the

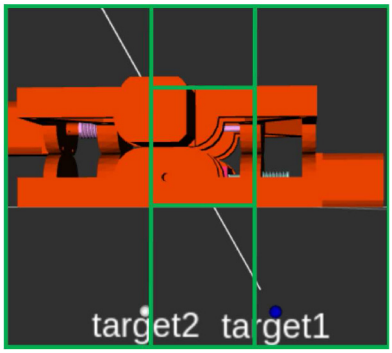

Fig. 6. Area division of the visual range.

support structure as follows:

$$\begin{cases} \Delta y = \dfrac{l}{\tan\theta_{\text{target}}} \\ y_{\text{low}} = \dfrac{l}{\tan\theta_{\text{boundary}}}, \quad \text{if } \theta_{\text{boundary}} < \theta_{\text{target}} \\ y_{\text{high}} = \Delta y - y_{\text{low}}. \end{cases} \tag{13}$$

Through (13), y_{low} and y_{hight} are the joint parameters that the robot needs to move. Similarly, the value of x_{low} and x_{high} can be obtained by analyzing the kinematics in tge XZ plane, and y_{hight} and x_{high} are compensated by changing the relative position of the support structure. Then, the puncture sheath can move to the desired pose according to Δy, Δx, and (8).

III. Eye-Gaze-Tracking-Based Control Approach

A. Eye-Gaze Tracking Framework

Controlling surgical robots with manual intervention is more complicated. In order to increase the intensity of the human–computer interaction, an eye-gaze tracking method has attracted much research attentions recently. Zhang *et al.* [32] constructed an eye-gazing system, which aims to benefit the disabled person by selecting the desired area via staring. Li *et al.* [31] used eye gaze to control the movement of the surgical robot and zoom in with specific areas. Li *et al.* [33] presented a low-cost, robust deep learning control surgical robot based on a gaze estimator.

Motivated to provide additional intuitive control approach for the puncture needle robot, an eye-gaze-based control approach is employed in this article. As shown in Fig. 6, the entire visualization area is divided into five main parts, i.e., left, right, up, down, and middle directions. To simplify the analysis, the upper and lower left corners are not considered and thus are included into the left region; similarly, the upper and lower right corners are included into the right section. The purpose of this design is to control the puncture needle position to the left and right when the eye-gaze direction moves to the corresponding directions. And the upper and lower direction is supposed to control the puncture needle to insert or retract.

The accurate eye-gaze direction estimation algorithm is crucial to achieve the eye-gaze-based control approach for the robot. The workflow of the eye-gaze direction estimation approach can be expressed in Fig. 7. First, the user's photograph is acquired by the camera, and the face detection method

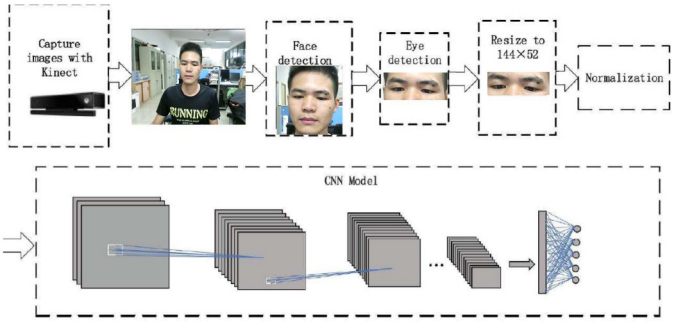

Fig. 7. Workflow of eye-gaze direction estimation algorithm.

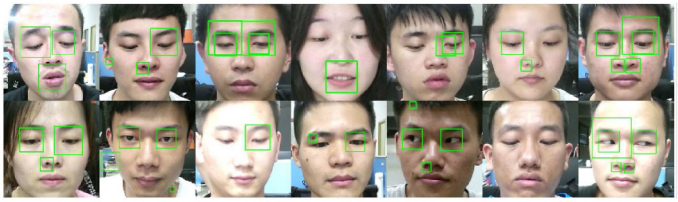

Fig. 8. Failed detection using Adaboost method.

is utilized to obtain the face image. Then, eye detection is performed based on the face image, which is normalized and resized to the size of 144 × 52. Following this, the convolutional neural network is used to obtain the corresponding features. And in the end, with the fully connected layer, Softmax is utilized to classify the gaze directions. Detailed installation is provided in the following sections.

B. Eye Detection Method

Li *et al.* [31] and Zhang *et al.* [32] used the Haar feature-based AdaBoost method [34] to detect eyes. However, we found that this method is quite sensitive to the environment, such as skin color, or light intensity, which may cause the detection errors as shown in Fig. 8. To address the sensitive issue of the above-mention method, further improved approach for eye detection needs to be designed or utilized. The geometric relationships between face features (such as eye, eyebrow, nose, mouth, etc.) are almost constant, and the photographs will not change these relationships when users facing the camera. Hence, there exists a certain relationship between the position of eyes and the boundaries of the face, which could be used to get the images of the eye area. On the other hand, standard image registration techniques using rigid affine model can be exploited to recover the position of the features as long as the eye gaze still appears in the vision scope during the tracking. This way, the eye-gaze tracking still works well even if the user does not face the camera directly.

To get the function of the eye position and the boundary of the face, the least-squares algorithm is used. The face image obtained through the face recognition method is square with side length as a. Thus, the position of the eye is assumed as the function of the side length of the face as follows:

$$Y_{\text{eye}} = D\eta \tag{14}$$

Fig. 9. Detection performance using the proposed method.

where $Y_{\text{eye}} = [x_{\text{eye1}} \quad x_{\text{eye2}} \quad y_{\text{eye1}} \quad y_{\text{eye2}}]^T$ is the coordinate of the eye region; $\eta = [a^2 \quad a \quad 1]^T$; and D is the coefficient matrix. Six hundred sets of existing data are used to fit the above method using the least squares, thereby obtaining a specific function expression. The experimental results verified the satisfactory performance, and some detection examples are shown in Fig. 9.

C. Data Collection and Augmentation

In the data collection step, a camera is used to collect the video of the eye gaze with five directions (up, down, left, right, and center) from 20 subjects, then the face detection algorithm and eye detection algorithm are used to obtain the region of eyes. In order to make the network more robust with different training data under various conditions, the data augmentation technique is utilized during the experiments to get additional training data set.

The data augmentation technique mainly considers image horizontal flipping, changing brightness, Gaussian noise, and image rotation. The image horizontal flipping can create numerous data. For example, when the original eye-gaze direction is left, the direction will be changed to the right after flipping. In this case, the augmented data will be considered with the right direction. Brightness of the collected image can be tuned to mimic the different lighting conditions, thus the model can be adapted to various environment and further to improve the performance under different lighting conditions. Considering the image sharpness, as well as the data generalization, the Gaussian noise is necessary to be considered during the training data collections. With respect to the different tilt angles of the human head, it is also important to take into account of the image rotations. It should be mentioned that only the case of $\pm 7°$ is considered in this article, and the tilt angle should be constrained within the predefined range of the practical implementations. The performance before and after using the augmentation method on the corresponding data is shown in Fig. 10.

D. Network Structure and Loss Function

Driven to prevent the model from degrading and speed up the convergence of the training, Resnet18 [35] architecture shown in Fig. 11 is used as the image feature extraction network, which consists of a series of residual blocks, not mention that this model can also extract features with improved efficiency. In our design, the input is the normalized human eye image with the size of 144×52, and the output is the features of the images.

Additive angular margin loss is used as the loss function that is proposed by Deng *et al.* [35], due to its advantage that can effectively reduce the intraclass distance while increasing the interclass distance, thus forming decision margin and

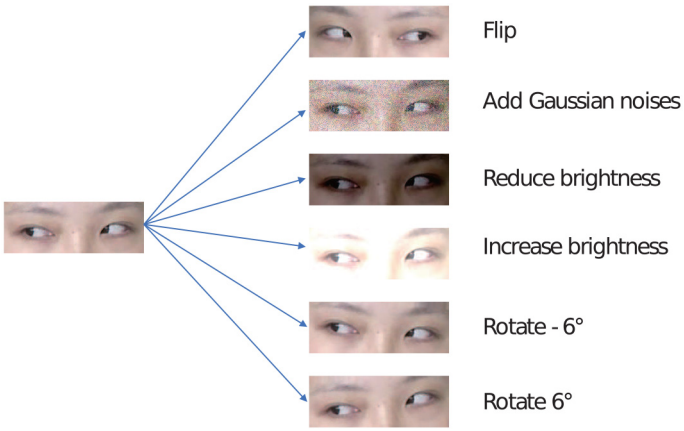

Fig. 10. Image data augmentation.

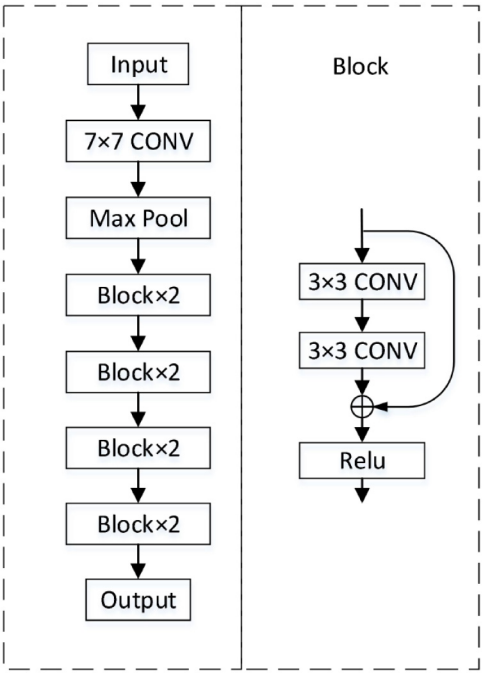

Fig. 11. Network structure of Resnet18. Resnet contains the residual structure shown on the right. Many experiments have proved that Resnet can effectively prevent the model from degrading, speed up the convergence, and facilitate the extraction of image features.

improving the classification accuracy and robustness. The loss function is modified on the basis of Softmax loss with the following form:

$$L_{\text{gaze}} = -\frac{1}{N}\sum_{i=1}^{N}\log\frac{e^{s(\cos(\theta_{y_i}+m))}}{e^{s(\cos(\theta_{y_i}+m))}+\sum_{j,j\neq y_i}^{n}e^{s\cos\theta_j}} \tag{15}$$

where s is the hypersphere radius that can be set as a constant value and has no influence of the classification; $\theta_{y_i} = \arccos([w_j/\|w_j\|] * [x_i/\|x_i\|])$, w_j denotes the weight of the jth class, referring to the class center of the jth class; x_i represents the feature of the ith training sample belonging to the jth class; and θ_{y_i} is the angle between the ith sample and the class center of the jth class. Additive angular margin loss adds a margin m to the original angle θ_{y_i}. The overall effect is to make the loss L_{gaze} larger and force the network to

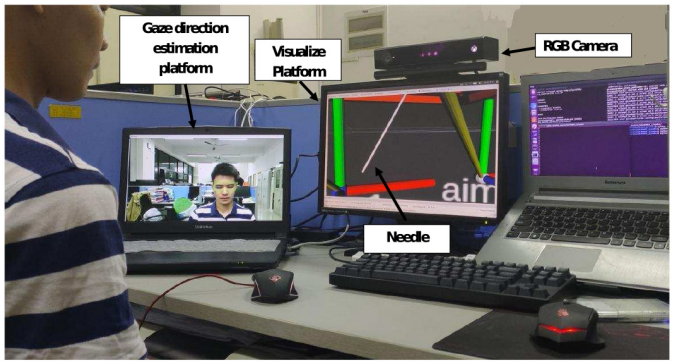

Fig. 12. Eye-gaze-tracking-based control experiment.

reduce the intraclass distance while increasing the interclass distance. Thus, highly discriminative features will be obtained to improve the accuracy of the classification.

IV. Experiments and Results

A. Experimental Setup

The experimental studies were conducted with simulation environment based on Gazebo and Rviz. First, the unified robot description format (URDF) derived from solid-works is used to develop the robotic structure, which mainly describes the coordinate transformation relationships of the robot and the outer structures of the robot. Fig. 12 provides the experimental setup in which a volunteer is controlling the robot through eye gaze. An RGB camera is utilized to capture the facial information of the user, and the eye-gaze tracking approach is applied to further obtain the eye-gaze direction. However, the surgeon or operator might make unintentional eye movement during the operation, which likely causes errors during the detection of the eye-gaze direction. Therefore, a soft safety switch is designed with the threshold d_{thr} of the relative position between the needle and the target point. Noted that d_{thr} should be smaller than or equal to the distance that the surgeon or operator normally moves the needle after it is positioned. In case that the distance exceeds d_{thr} or the gaze tracking failed, the surgeon is able to manually tune the needle position though the soft safety switch. Fig. 13 shows the control performance of the robot when locating different targets.

During the simulation configurated experiments that use Rviz visualization environment, the motion model should be finalized to set the physical environment. In our experimental studies, the Gazebo is used to build simulated puncture operation environment. Several target points with different sizes are designed, and the robot can be controlled through the eye-gaze system to further rotate the puncture sheath. When the rotation angle of the puncture sheath is fixed, the needle can be controlled to insert or retract following the desired direction of the puncture sheath coordinate system. However, it is not easy to guarantee the motion state of the robot in the ideal state consistent with the one of the simulated robot generated by Gazebo. Hence, it is necessary to establish the robot structure in the ideal state through the kinematic model on Rviz and then to control the robot within the ideal state.

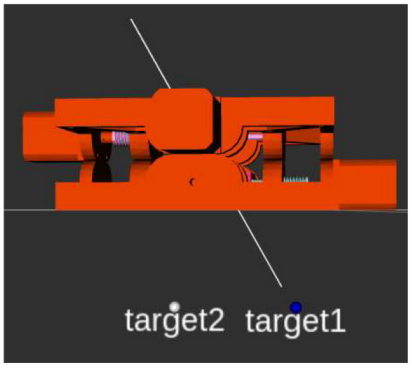

(a)

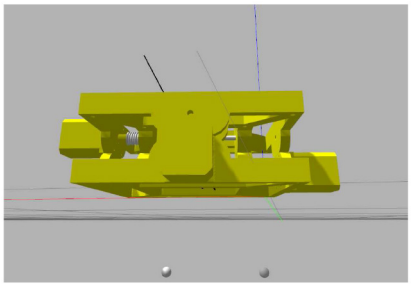

(b)

Fig. 13. Both simulation platforms run simultaneously. (a) Robot moves under the received ROS messages at Gazebo simulation platform. The parameters of the robot model can be defined on the platform. (b) Rviz robot visualization platform also controls the robot through ROS messages, but only through coordinate transformation.

To verify the effectiveness of the eye-gaze tracking method for controlling the robot to reach the desired target, the distance from the end effector of the robot to the target point is also considered. The accuracy results are shown in Table II. Assume that the horizontal height of the needle is H, meanwhile, a reachable target and a random target are also designed for the experiment within the working space range of the robot. Due to the rotation of the needle, it is hard to reach the random target point without the manual intervention. In order to obtain the advantages and disadvantages of different methods applied in the medical environment, Euclidean distance d_i between the target point to the needle position is calculated, and the average is derived as $E = d_i/N_i$.

B. Result Analysis

In the experimental studies, first five gaze directions (up, down, left, right, and middle) are used in the training set of the eye images (with the amount in total of 10 094). During the training step, the batch size is set as 32, the learning rate is set to 0.0001, and the Adam method [36] is used for optimization until the loss value is stable. In order to verify the performance of the learning method, two-loss functions (Softmax loss and additive angle margin loss) were used, and two models for gaze direction classification were obtained. It is observed from the experiments that the training model with additive angular margin loss function achieves higher accuracy while the additional angle m is set to 0.5.

TABLE I
COMPARISON OF THE CLASSIFICATION ACCURACY OF BOTH MODELS UNDER TEST SET 1 TEST SET 2

Loss function	Accuracy(%)		Accuracy difference(%)
	Test Set 1	Test Set 2	
Angular Margin Loss	99.55	91.96	7.59
Softmax Loss	94.76	77.53	17.23

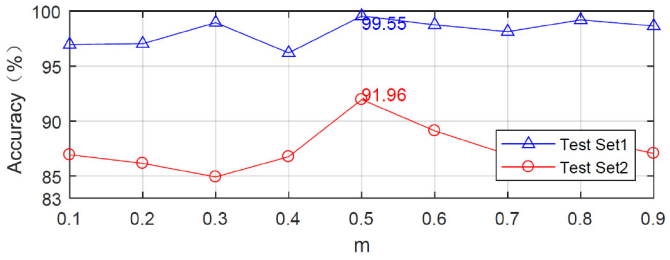

Fig. 14. Classification accuracy of the model in two test sets when m is different. Among them, the model can obtain the highest classification accuracy in both test sets when $m = 0.5$.

Further tests were performed with two data sets, indicated as Test Set 1 and Test Set 2, in which Test Set 2 was derived by the image blur based on the Test Set 1. The reason for using two data sets is that the images collected from the RGB camera are clear, and the Test Set 2 is designed to evaluate two different loss functions for the model. The results of the tests with the two models are provided in Table I.

Since it is noticed that the additional angle m in additive angular margin loss has certain influence on the classification, and the m is usually chosen to be greater than 0 and cannot be oversized. In the experimental studies, a series of m ranged from 0.1 to 0.9 are utilized to train the different models. The results are shown in Fig. 14, and it is noticed that the accuracy of angular margin loss is higher than the one using the Softmax loss function.

To further analyze the experimental result, it can be observed from Fig. 14 and Table I that the model trained with additive angular margin loss function has higher accuracy in both Test Set than the model trained with the Softmax loss function regardless of the value of m. It should also be emphasized that the accuracy of the models with Test Set 2 is lower than that of Test Set 1. The reason is that the image used in Test Set 2 are fuzzified with significant difference from the training data set. The accuracy of the model trained with additive angular margin loss function decreases by 7.59%, while the model trained with the Softmax loss function decreases by 17.23%. This is mainly because the additive angular margin loss function is capable of making the network to reduce the intraclass distance and increase the interclass distance so that to improve the overall accuracy of classification. From the performance comparisons, the additive angular margin loss function is utilized for the eye-gaze direction classification for the designed robot system.

In Table II, the results of the distance accuracy are also provided. The selected data are all sampling point within 18 mm from the target. $E_{\text{reachable}}$ represents the average Euclidean distance to the reachable target, and E_{random} represents the one to the random target. Two classification models mentioned in the previous section are used, and it is observed that the angular margin loss function model has almost twice accuracy when compared with the Softmax loss function mode during the experimental setup with reachable target. While in the case of approaching the same random target, the accuracy of the angular margin loss function also has enhanced performance. The result again presents that the angular margin loss function is capable of providing better performance for the designed robotic system with eye-gaze-tracking-based control.

TABLE II
ACCURACY MEASURE OF THE ROBOT CONTROL SYSTEM

Loss function	Angular Margin Loss	Softmax Loss
$E_{reachable}(mm)$	0.6773	1.2095
$E_{random}(mm)$	1.3014	1.7029

V. CONCLUSION

In this article, a novel robot system was designed to enable percutaneous needle guidance with consideration of the clinical application. The robot operating system (ROS)-based virtual platform was implemented with the designed robotic system for needle positioning. An eye-gaze-tracking-based control framework is developed to control the robot with desired needle positioning, thus the clinician is capable of controlling the direction of the puncture sheath of the robot to reach the target by means of eye gaze. Experimental studies have been conducted to verify the effectiveness of the designed platform with the proposed eye-gaze-tracking-based control approach. The results showed that the designed robot can be controlled through the eye-gaze tracking method and guided to the desired target at the average error of 1 mm.

Future work will focus on the following aspects.

1) Prototypes of the robotic systems will be designed and manufactured for real experiments.
2) More factors of the eye gaze tracking-based robotic motion control will be considered, such as errors in the eye gaze direction detection caused by the fatigueness.
3) *In vivo*/*vitro* experiments with the clinical environment will be performed.
4) Reinforcement learning-based path planning [37] will be studied for the movement of the needle.

ACKNOWLEDGMENT

The gaze tracking algorithm code has been uploaded to Github: https://github.com/txwhqq/Eye-gaze-estimation.

REFERENCES

[1] L. B. Kratchman, M. M. Rahman, J. R. Saunders, P. J. Swaney, and R. J. Webster, III, "Toward robotic needle steering in lung biopsy: A tendon-actuated approach," in *Proc. Med. Imaging Vis. Image Guided Procedures Model.*, vol. 7964, 2011, Art. no. 79641I.

[2] Y. Chen *et al.*, "MRI-guided robotically assisted focal laser ablation of the prostate using canine cadavers," *IEEE Trans. Biomed. Eng.*, vol. 65, no. 7, pp. 1434–1442, Jul. 2018.

[3] Y. Chen *et al.*, "Design and fabrication of MR-tracked metallic stylet for gynecologic brachytherapy," *IEEE/ASME Trans. Mechatronics*, vol. 21, no. 2, pp. 956–962, Apr. 2016.

[4] J. M. Fitzpatrick, J. B. West, and C. R. Maurer, "Predicting error in rigid-body point-based registration," *IEEE Trans. Med. Imag.*, vol. 17, no. 5, pp. 694–702, Oct. 1998.

[5] J. Ghelfi *et al.*, "Evaluation of the needle positioning accuracy of a light puncture robot under MRI guidance: Results of a clinical trial on healthy volunteers," *Cardiovasc. Interv. Radiol.*, vol. 41, no. 9, pp. 1428–1435, 2018.

[6] R. Monfaredi, K. Cleary, and K. Sharma, "MRI robots for needle-based interventions: Systems and technology," *Ann. Biomed. Eng.*, vol. 46, no. 3, pp. 1479–1497, 2018.

[7] N. Hungr, I. Bricault, P. Cinquin, and C. Fouard, "Design and validation of a CT- and MRI-guided robot for percutaneous needle procedures," *IEEE Trans. Robot.*, vol. 32, no. 4, pp. 973–987, Aug. 2016.

[8] W. J. Heerink *et al.*, "Robotic versus freehand needle positioning in CT-guided ablation of liver tumors: A randomized controlled trial," *Radiology*, vol. 290, no. 3, pp. 826–832, 2019.

[9] A. Squires, J. N. Oshinski, N. M. Boulis, and Z. T. H. Tse, "SpinoBot: An MRI-guided needle positioning system for spinal cellular therapeutics," *Ann. Biomed. Eng.*, vol. 46, no. 3, pp. 475–487, 2018.

[10] T. Hiraki *et al.*, "Robotically driven CT-guided needle insertion: Preliminary results in phantom and animal experiments," *Radiology*, vol. 285, no. 2, pp. 454–461, 2017.

[11] T. Hiraki, T. Kamegawa, T. Matsuno, T. Komaki, J. Sakurai, and S. Kanazawa, "Zerobot: A remote-controlled robot for needle insertion in CT-guided interventional radiology developed at Okayama University," *Acta Medica Okayama*, vol. 72, no. 6, pp. 539–546, 2018.

[12] K. Y. Kim, H. S. Woo, J. H. Cho, and Y. K. Lee, "Development of a two DOF needle driver for CT-guided needle insertion-type interventional robotic system," in *Proc. 26th IEEE Int. Symp. Robot Human Interact. Commun. (RO-MAN)*, Aug. 2017, pp. 470–475.

[13] A. Melzer *et al.*, "INNOMOTION for percutaneous image-guided interventions," *IEEE Eng. Med. Biol. Mag.*, vol. 27, no. 3, pp. 66–73, May/Jun. 2008.

[14] E. G. Christoforou, I. Seimenis, E. Andreou, E. Eracleous, and N. V. Tsekos, "A novel, general-purpose, MR-compatible, manually actuated robotic manipulation system for minimally invasive interventions under direct MRI guidance," *Int. J. Med. Robot. Comput. Assist. Surg. Mrcas*, vol. 10, no. 1, pp. 22–34, 2014.

[15] D. Y. Song *et al.*, "Robotic needle guide for prostate brachytherapy: Clinical testing of feasibility and performance," *Brachytherapy*, vol. 10, no. 1, pp. 57–63, 2011.

[16] B. Schulz *et al.*, "Accuracy and speed of robotic assisted needle interventions using a modern cone beam computed tomography intervention suite: A phantom study," *Eur. Radiol.*, vol. 23, no. 1, pp. 198–204, 2013.

[17] M. H. Loser and N. Navab, "A new robotic system for visually controlled percutaneous interventions under CT fluoroscopy," in *Proc. Med. Image Comput. Comput. Assist. Interv. (MICCAI)*, 2000, pp. 887–896.

[18] B. Schell *et al.*, "Robot-assisted biopsies in a high-field MRI system-first clinical results," *RoFo Fortschritte auf dem Gebiete der Rontgenstrahlen und der Nuklearmedizin*, vol. 184, no. 1, pp. 42–47, 2012.

[19] D. Stoianovici, L. L. Whitcomb, J. H. Anderson, R. H. Taylor, and L. R. Kavoussi, "A modular surgical robotic system for image guided percutaneous procedures," in *Proc. Int. Conf. Med. Image Comput. Comput. Assist. Interv.*, 1998, pp. 404–410.

[20] H. Su, C. Yang, G. Ferrigno, and E. De Momi, "Improved human–robot collaborative control of redundant robot for teleoperated minimally invasive surgery," *IEEE Robot. Autom. Lett.*, vol. 4, no. 2, pp. 1447–1453, Apr. 2019.

[21] C. Yang, C. Chen, N. Wang, Z. Ju, J. Fu, and M. Wang, "Biologically inspired motion modeling and neural control for robot learning from demonstrations," *IEEE Trans. Cognitive Dev. Syst.*, vol. 11, no. 2, pp. 281–291, Jun. 2019.

[22] C. Yang, X. Wang, L. Cheng, and H. Ma, "Neural-learning-based telerobot control with guaranteed performance," *IEEE Trans. Cybern.*, vol. 47, no. 10, pp. 3148–3159, Oct. 2017.

[23] C. Yang, J. Luo, Y. Pan, Z. Liu, and C.-Y. Su, "Personalized variable gain control with tremor attenuation for robot teleoperation," *IEEE Trans. Syst., Man, Cybern., Syst.*, vol. 48, no. 10, pp. 1759–1770, Oct. 2018.

[24] C. Yang, X. Wang, Z. Li, Y. Li, and C.-Y. Su, "Teleoperation control based on combination of wave variable and neural networks," *IEEE Trans. Syst., Man, Cybern., Syst.*, vol. 47, no. 8, pp. 2125–2136, Aug. 2017.

[25] H. Su, J. Sandoval, P. Vieyres, G. Poisson, G. Ferrigno, and E. De Momi, "Safety-enhanced collaborative framework for tele-operated minimally invasive surgery using a 7-DoF torque-controlled robot," *Int. J. Control Autom. Syst.*, vol. 16, no. 6, pp. 2915–2923, 2018.

[26] H. Su, J. Sandoval, M. Makhdoomi, G. Ferrigno, and E. De Momi, "Safety-enhanced human–robot interaction control of redundant robot for teleoperated minimally invasive surgery," in *Proc. IEEE Int. Conf. Robot. Autom. (ICRA)*, 2018, pp. 6611–6616.

[27] J. Guo, C. Liu, and P. Poignet, "A scaled bilateral teleoperation system for robotic-assisted surgery with time delay," *J. Intell. Robot. Syst.*, vol. 95, no. 1, pp. 165–192, 2019.

[28] G. Jing, L. Ping, H. Yan, and H. Ren, "Viscoelastic model based bilateral teleoperation for robotic-assisted tele-palpation," *Assembly Autom.*, vol. 37, no. 3, pp. 322–334, 2017.

[29] C. Liu, J. Guo, and P. Poignet, "Nonlinear model-mediated teleoperation for surgical applications under time variant communication delay," *IFAC-PapersOnLine*, vol. 51, no. 22, pp. 493–499, 2018.

[30] H. M. Yip, D. Navarro-Alarcon, and Y.-H. Liu, "An image-based uterus positioning interface using ADALINE networks for robot-assisted hysterectomy," in *Proc. IEEE Int. Conf. Real Time Comput. Robot.*, 2018, pp. 182–187.

[31] P. Li, X. Hou, X. Duan, H. Yip, G. Song, and Y. Liu, "Appearance-based gaze estimator for natural interaction control of surgical robots," *IEEE Access*, vol. 7, pp. 25095–25110, 2019.

[32] C. Zhang, R. Yao, and J. Cai, "Efficient eye typing with 9-direction gaze estimation," *Multimedia Tools Appl.*, vol. 77, no. 15, pp. 19679–19696, 2018.

[33] P. Li, X. Hou, L. Wei, G. Song, and X. Duan, "Efficient and low-cost deep-learning based gaze estimator for surgical robot control," in *Proc. IEEE Int. Conf. Real Time Comput. Robot. (RCAR)*, 2018, pp. 58–63.

[34] P. Viola and M. Jones, "Rapid object detection using a boosted cascade of simple features," in *Proc. IEEE Comput. Soc. Conf. Comput.Vis. Pattern Recognit. (CVPR)*, vol. 1, Dec, 2001, pp. 511–518.

[35] J. Deng, J. Guo, N. Xue, and S. Zafeiriou, "ArcFace: Additive angular margin loss for deep face recognition," in *Proc. IEEE Conf. Comput. Vis. Pattern Recognit.*, 2019, pp. 4690–4699.

[36] D. P. Kingma and J. Ba, "Adam: A method for stochastic optimization," *arXiv:cs.LG/1412.6980*, 2014.

[37] Z. Cao, H. Guo, J. Zhang, F. Oliehoek, and U. Fastenrath, "Maximizing the probability of arriving on time: A practical Q-learning method," in *Proc. 31st AAAI Conf. Artif. Intell.*, 2017, pp. 4481–4487.

Jing Guo received the bachelor's and master's degrees from the Guangdong University of Technology, Guangzhou, China, in 2009 and 2012, respectively, and the Ph.D. degree from the University of Montpellier, Montpellier, France, in 2016.

He has been a Research Fellow with the National University of Singapore, Singapore, from 2016 to 2018. He is currently affiliated with the Guangdong University of Technology. His current research interests include robotic control, haptic bilateral teleoperation, and surgical robotics.

Yi Liu received the bachelor's degree in automation from the Guangdong University of Technology, Guangzhou, China, in 2018, where he is currently pursuing the M.S. degree.

His research and interests include robotic intelligent control, machine learning, and human–computer interaction.

Qing Qiu received the bachelor's degree in electronic information science and technology from the Guangdong University of Technology, Guangzhou, China, in 2018, where he is currently pursuing the M.S. degree.

His research interests include computer vision and machine learning.

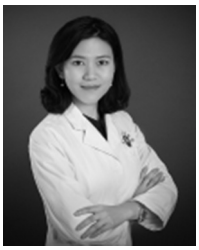

Jie Huang received the Ph.D. degree in oncology from Southern Medical University, Guangzhou, China, in 2016.

She joined the Guangdong Lung Cancer Institute, Guangdong Provincial People's Hospital, Guangzhou, as a Clinical Doctor in 2016. She is involved in several national research projects as a Principle Investigator or participant. Her research interests include immunotherapy, target therapy, and their resistance mechanisms in lung cancer.

Chao Liu (Senior Member, IEEE) received the Ph.D. degree in electrical and electronic engineering from Nanyang Technological University, Singapore, in 2006.

He joined French National Center for Scientific Research (CNRS), Montpellier, France, as a CR2 Research Scientist in 2008 and was promoted to a CR1 Senior Research Scientist in 2012. He is involved in several European and French national research projects on medical robotics as a Principle Investigator or participant. His research interests include surgical robotics, teleoperation, haptics, control theory/system, and computer vision.

Dr. Liu is an Expert Panelist of Project Evaluation Committee for French National Research Agency (ANR) and Swiss National Science Foundation. He has been serving on the IEEE Technical Committee on "Telerobotics" since 2011, the IFAC Technical Committee on "Biological and Medical systems" since 2012, and the IEEE Technical Committee on "Haptics." He also serves as a program committee member and an associate editor for numerous international conferences.

Zhiguang Cao received the B.Eng. degree in automation from the Guangdong University of Technology, Guangzhou, China, in 2009, the M.Sc. degree in signal processing from Nanyang Technological University, Singapore, in 2012, and the Ph.D. degree from the Interdisciplinary Graduate School, Nanyang Technological University, in 2017.

He has been a Research Fellow with Future Mobility Research Lab, and Energy Research Institute @ NTU (ERI@N), Singapore, since 2016. He is currently a Research Assistant Professor with the Department of Industrial Systems Engineering and Management, National University of Singapore, Singapore. His research interests include the application of AI and optimization for intelligent systems.

Yue Chen (Member, IEEE) received the B.S. degree in vehicle engineering from Hunan University, Hunan, China, in 2010, the M.Phil. degree in mechanical engineering from Hong Kong Polytechnic University, Hong Kong, in 2013, and the Ph.D. degree in mechanical engineering from Vanderbilt University, Nashville, TN, USA, in 2018.

He started an Assistant Professor position with the Department of Mechanical Engineering, University of Arkansas, Fayetteville, AR, USA, in 2018. His current research interests include medical robotics and soft robots.